

See discussions, stats, and author profiles for this publication at: <https://www.researchgate.net/publication/41577072>

Influence of Biomacromolecules and Humic Acid on the Aggregation Kinetics of Single-Walled Carbon Nanotubes

ARTICLE *in* ENVIRONMENTAL SCIENCE AND TECHNOLOGY · FEBRUARY 2010

Impact Factor: 5.33 · DOI: 10.1021/es903059t · Source: PubMed

CITATIONS

155

READS

84

3 AUTHORS, INCLUDING:



[Navid B Saleh](#)

University of Texas at Austin

68 PUBLICATIONS 3,242 CITATIONS

[SEE PROFILE](#)



[Menachem Elimelech](#)

Yale University

394 PUBLICATIONS 32,588 CITATIONS

[SEE PROFILE](#)

Influence of Biomacromolecules and Humic Acid on the Aggregation Kinetics of Single-Walled Carbon Nanotubes

NAVID B. SALEH,^{*,†} LISA D. PFEFFERLE,[‡] AND MENACHEM ELIMELECH[‡]

Department of Civil and Environmental Engineering, University of South Carolina, Columbia, South Carolina 29208, and Department of Chemical Engineering, Environmental Engineering Program, Yale University, New Haven, Connecticut 06520-8286

Received October 7, 2009. Revised manuscript received February 1, 2010. Accepted February 4, 2010.

The initial aggregation kinetics of single-walled carbon nanotubes (SWNTs) were studied using time-resolved dynamic light scattering. Aggregation of SWNTs was evaluated in the presence of natural organic matter [Suwannee River humic acid (SRHA)], polysaccharide (alginate), protein [bovine serum albumin (BSA)], and cell culture medium [Luria-Bertani (LB) broth] with varying solution concentrations of monovalent (NaCl) and divalent (CaCl_2) salts. Increasing salt concentration and adding divalent calcium ions induced SWNT aggregation by screening electrostatic charge and thereby suppressing electrostatic repulsion, similar to observations with aquatic colloidal particles. The presence of biomacromolecules significantly retarded the SWNT aggregation rate. BSA protein molecules were most effective in reducing the rate of aggregation followed by SRHA, LB, and alginate. The slowing of the SWNT aggregation rate in the presence of the biomacromolecules and SRHA can be attributed to steric repulsion originating from the adsorbed macromolecular layer. The remarkably enhanced SWNT stability in the presence of BSA, compared to that with the other biomacromolecules and SRHA, is ascribed to the BSA globular molecular structure that enhances steric repulsion. The results have direct implications for the fate and behavior of SWNTs in aquatic environments and biological media.

Introduction

Hexagonal carbon lattices folded to helicoidal tubular structures, called carbon nanotubes, have exceptional physicochemical properties and are one of the most prevalent nanomaterials. Single-walled carbon nanotubes (SWNTs), the one-dimensional allotrope of this carbon molecule structure, are now being mass produced in metric ton quantities with a projected production rate of 21.7 t/year (1). The commercial sector has realized the industrial application potential of SWNTs in nanocomposites, field emission devices, and energy storage (2). SWNTs are also being increasingly used as a new biosensor material (3) and as a

novel vehicle for translocating therapeutic molecules for drug delivery (4). This increased production rate and use of SWNTs in commercial products make it more likely that raw SWNT discharge or SWNTs from discarded SWNT-laden products will be released into natural aquatic and biological environments.

A SWNT is a unique solid state material that has all of its atoms on the surface. The interfacial chemistry of SWNTs, namely, the type of functional groups and adsorbed molecules on the SWNT, is critical for its colloidal stability and, therefore, its behavior in natural and biological environments (5). Upon introduction of SWNTs into natural and biological environments, SWNTs will interact with natural organic matter and biological macromolecules and, thus, are likely to undergo surface modification (3, 6, 7). The interplay between the universal van der Waals attraction and steric repulsion originating from the adsorbed macromolecular layers is expected to have a profound impact on SWNT aggregation kinetics.

SWNTs will exist in various aggregation states when introduced into natural and biological environments, which will influence their interaction with mineral surfaces and biological species. The propensity of SWNTs to aggregate under various solution conditions necessitates a systematic study of the aggregation kinetics with the macromolecules of environmental and biological relevance. Most of the literature to date has focused on the overall stability and solubilization of carbon nanotubes using covalent and noncovalent functionalization (8–12). There is a paucity of published studies concerning the fundamental aggregation kinetics of carbon nanotube suspensions, particularly those of SWNTs. To date, only multiwalled carbon nanotubes (MWNTs) have been systematically evaluated for their aggregation (9, 12, 13), demonstrating that MWNT aggregation behavior is in principle similar to that of most aqueous colloidal materials (9, 13). The literature on SWNT stability focuses on overall aggregate structures of SWNTs and employs qualitative solution depletion techniques to evaluate SWNT stability (14–17).

Because of their hydrophobic surface properties, SWNTs readily associate with biological macromolecules, such as proteins (18–20) and antibodies (21), as well as natural organic matter, such as humic substances (6). The interaction of SWNTs with macromolecules is inevitable in biological and environmental systems. Applications of SWNTs in biological systems often involve culture media that contain biomacromolecules, such as enzymes, proteins, DNA, and polysaccharides. Likewise, studies or applications of SWNTs in environmental systems will result in interactions of SWNTs with humic substances, which are ubiquitous in the environment. The presence of macromolecules can influence the aggregation behavior of SWNTs and thereby their interaction with biological species and natural interfaces. There have been no studies to date that focus systematically on the role of biomacromolecules and humic acid in the aggregation behavior of carbon nanotubes.

The objective of this paper is to investigate the effect of biomacromolecules and humic acid on the aggregation kinetics of SWNTs under various solution chemistries. The biomacromolecules used include a polysaccharide (sodium alginate), a protein [bovine serum albumin (BSA)], a microbial culture medium [Luria-Bertani (LB) broth], and a humic acid [Suwannee River humic acid (SRHA)]. Solution chemistry variations include monovalent (NaCl) and divalent (CaCl_2) salt concentrations. SWNT stability curves were constructed using the aggregation kinetics data from which the critical coagulation concentrations for the monovalent and divalent

* Corresponding author email: salehn@engr.sc.edu; phone: 803-777-2288.

[†] University of South Carolina.

[‡] Yale University.

salts were determined. The measured physicochemical properties of SWNTs are used to elucidate the aggregation mechanisms with biomacromolecules and humic acid.

Materials and Methods

Preparation of SWNTs. We used commercially available SWNTs (Cheap Tubes Inc., Brattleboro, VT). The supplier reports that more than 90% by mass is SWNT with a bulk density of 2.1 g/cm³ at 20 °C. It is also reported that the SWNTs are on average 0.8–1.6 nm in diameter and 5–30 μm in length. The SWNTs were independently characterized in this study.

The SWNT samples for aggregation experiments were prepared using a successive sonication and clarification technique as described in our previous aggregation kinetics study with multiwalled carbon nanotubes (MWNTs) (13). In short, 50 mg of as-received (untreated) SWNT powder was added to 500 mL of deionized water (Barnstead), and the mixture was sonicated continuously using an ultrasonication probe (Misonix 3000, Misonix Inc., Farmingdale, NY) for 30 min. The SWNT suspension was then left aside quiescently at room temperature for 10 min, and the stable supernatant was collected. The collected supernatant was resonicated following the same procedure for six additional cycles. The final collected SWNT stock was stable for the duration of all the aggregation experiments.

Characterization of SWNTs. SWNT samples were characterized for purity and key physicochemical properties for both the as-received (untreated) and sonicated (treated) samples. The electrophoretic mobility (EPM) measurements and imaging of tubes were conducted with samples from the same stock used for aggregation experiments. Raman spectroscopy and thermogravimetric analysis (TGA) require a greater mass of samples. To obtain significant mass to perform these measurements, we prepared a new stock using seven cycles of successive sonication, but the entire mass of SWNTs was retained throughout the duration of the sonication treatment.

The electrophoretic mobilities of SWNT samples were measured for a range of salt concentrations in the presence of the biomacromolecules (i.e., alginate, BSA, and LB) and SRHA with the ZetaPALS analyzer (Brookhaven Instrument Corp., Holtsville, NY) at 24 °C. For these measurements, the SWNT suspension was diluted by a factor of 5 from the stock prepared for the aggregation experiments. Salt solutions and biomacromolecules or SRHA were added immediately prior to the EPM measurements to mimic the aggregation experiments. At least 30–40 measurements were taken for each solution condition.

A high-resolution transmission electron microscope (TEM) (Tecnai G2, FEI Co., Eindhoven, The Netherlands) was used to image SWNT samples. Aqueous suspensions of both the untreated and treated SWNTs were used from the stocks for aggregation experiments. A drop of the SWNT suspension was placed directly on a nickel TEM grid coated with carbon-Formvar and left to adsorb for 2 min. The excess water was then absorbed with a filter paper. For the TEM imaging of the SWNTs with alginate in the presence of CaCl₂, the aqueous sample was prepared following the procedure used in the aggregation experiment. The TEM grid was prepared 5 min after preparation of the aqueous sample.

Raman spectra were recorded with untreated and treated dry SWNT samples using a Jasco multiwavelength NRS-3000 series Raman spectrometer (Jasco Inc., Easton, MD) equipped with a confocal microscope, anastigmatic 300 mm focal length spectrograph, and a thermoelectrically cooled charge-coupled device (CCD). The integration time was 15 s for each spectrum, with each spectrum representing the average of five scans. The spectra were recorded at a wavelength of 785

nm (1.58 eV). It is to be noted that all the Raman spectra were recorded on dry SWNT samples.

The purity of the untreated SWNT samples was determined via thermogravimetric analysis (TGA) (SetSys 1750, Setaram Instrumentation, Caluire, France) using a holey crucible. An as-received SWNT sample of 14.21 g was used for TGA, where the sample was heated at a constant temperature ramp of 10 °C/min to 1000 °C in the presence of oxygen. The weight loss of the sample was monitored throughout the heating process.

Solution Chemistry. SWNT aggregation experiments were conducted with monovalent (NaCl) and divalent (CaCl₂) electrolyte solutions (reagent grade, J. T. Baker, Phillipsburg, NJ) over a wide concentration range. The pH of the SWNT suspensions at all salt concentrations was unadjusted (ambient) and determined to be 6.0 ± 0.2. All reagent solutions were filtered with 0.1 μm inorganic membrane filters (Anopore 25, Whatman, Middlesex, U.K.).

Biomacromolecules and Humic Acid. The biomacromolecules used for the aggregation experiments included a polysaccharide (alginate sodium salt, Sigma Aldrich), a protein (BSA, Sigma Aldrich), and a microbial culture medium (LB, Fisher Scientific). Suwannee River humic acid (SRHA) was used as a model natural organic matter (Standard II, International Humic Substances Society). We prepared the biomacromolecule and SRHA stock solutions (600 mg/L) by stirring the solutions overnight in the dark. The solutions were then filtered under vacuum using a 0.22 μm cellulose acetate membrane filter (Corning Inc., Corning, NY). All stock solutions were adjusted to pH 6.0 via addition of NaOH or HCl, and the stocks were subsequently stored in the dark at 4 °C. The total organic carbon (TOC) content of the biomacromolecules was found to be 31.8% for alginate, 47.4% for BSA, 24.7% for LB, and 50.78% for SRHA through high-temperature oxidation (TOC-V CSH, Shimadzu, Kyoto, Japan). The final biomacromolecule and SRHA concentration was maintained at 2.5 mg/L of TOC during the SWNT aggregation and characterization experiments.

SWNT Aggregation. The aggregation experiments were performed using a multiangle light scattering unit (ALV-5000, Langen). The details of the instrument and aggregation experiment protocol are described elsewhere (13, 22). In brief, the SWNT samples were placed in new glass vials (Supelco, Bellefonte, PA) that were thoroughly cleaned using a cleaning solution (Extran MA 01, Merck KGaA, Darmstadt, Germany). The SWNT samples for the aggregation experiments were diluted by a factor of 3 from the original stock. Electrolyte solutions and biomacromolecules or SRHA were added prior to the aggregation experiments following the protocol described by Saleh et al. (13) and Chen and Elimelech (22, 23). We first added the biomacromolecules and SRHA to the SWNT suspensions followed by salt additions. The dynamic light scattering measurements were conducted by positioning the detector at 90° from the incident laser beam, allowing the autocorrelation function to accumulate for 15 s. We performed the measurements for a time period ranging from 20 min to 3 h to obtain an approximately 30% increase in the original hydrodynamic radius of SWNTs.

The initial aggregation rate constant of SWNTs is proportional to the initial rate of increase in the hydrodynamic radius (R_h) with time (t) and the inverse of the SWNT concentration (N_0) (23):

$$k \propto \frac{1}{N_0} \left[\frac{dR_h(t)}{dt} \right]_{t=0} \quad (1)$$

Because the SWNT concentration in all aggregation experiments was identical, the attachment efficiency (α) is readily obtained by normalizing the initial slope of the

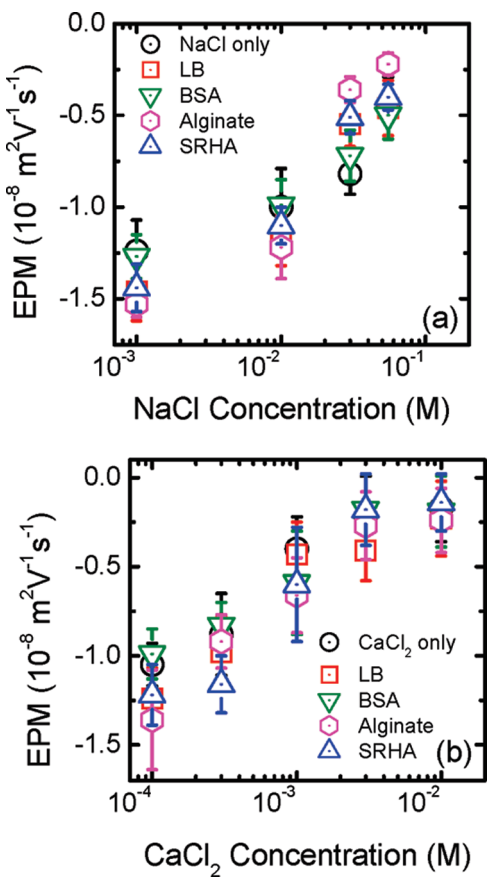


FIGURE 1. Electrophoretic mobility (EPM) of SWNTs in the presence of various biomacromolecules and Suwannee River humic acid (SRHA) as a function of (a) NaCl or (b) CaCl₂ concentration. The concentration of each macromolecule was maintained at 2.5 mg/L of total organic carbon (TOC). Measurements were taken at pH 6.0 and 24 °C.

aggregation profile at a given solution chemistry by the initial slope obtained for favorable (fast) aggregation conditions:

$$\alpha = \frac{\left[\frac{dR_h(t)}{dt} \right]_{t=0}}{\left[\frac{dR_h(t)}{dt} \right]_{t=0,\text{fav}}} \quad (2)$$

where the subscript fav represents favorable solution conditions, under which fast, diffusion-limited aggregation takes place. The slope for the fast aggregation conditions was determined from aggregation experiments at a high salt (NaCl or CaCl₂) concentration, above which the aggregation rate does not increase with an increase in salt concentration.

Results and Discussion

SWNT Characteristics. Figure 1 presents the electrophoretic mobility (EPM) of SWNTs as a function of salt concentration in the presence of biomacromolecules and humic acid. Measurements showed negative surface potential (charge) for SWNTs at pH 6.0, consistent with previously reported literature data for SWNTs (17, 24, 25) and MWNTs (9, 13, 26) in aqueous solutions. Increasing the monovalent and divalent salt concentration made the electrophoretic mobility (EPM) values less negative, from $-1.24 \times 10^{-8} \text{ m}^2 \text{ V}^{-1} \text{ s}^{-1}$ for 1 mM NaCl to $-0.46 \times 10^{-8} \text{ m}^2 \text{ V}^{-1} \text{ s}^{-1}$ for 55 mM NaCl, which is commonly observed with most colloidal particles in aqueous solutions. This range is consistent with the EPM of SWNTs measured by Sano et al. (17) ($-0.93 \times 10^{-8} \text{ m}^2 \text{ V}^{-1} \text{ s}^{-1}$) and Hu et al. (24) ($-0.8 \times 10^{-8} \text{ m}^2 \text{ V}^{-1} \text{ s}^{-1}$ at pH 8.0). The origin

of the surface charge of pristine carbonaceous nanomaterials (i.e., fullerenes, SWNTs, and MWNTs) is not well understood. It has been hypothesized that negative surface charge is incurred due to electron density distribution (27, 28) or accumulation of hydroxides over hydronium ions on the surface (29, 30). The surface potential can also be acquired by dissociation of surface functional groups that form by surface oxidation (9, 17, 31) or, as in this study, by mechanochemistry (11). Defect sites in carbon nanotubes can also create surface functional groups that may be responsible for the negative surface charge (13), which will be discussed later when the SWNT Raman spectra are presented. The presence of biomacromolecules and humic acid did not enhance the EPM of SWNTs significantly, with the most negative value ($-1.53 \times 10^{-8} \text{ m}^2 \text{ V}^{-1} \text{ s}^{-1}$) obtained for 1 mM NaCl in the presence of alginate. Literature data indicate that EPM of SWNTs can increase significantly with adsorbed surfactants and polyelectrolytes (32, 33).

TEM imaging indicates that the majority of the tubes are SWNTs, with some larger diameter tubes, most likely double-walled or multiwalled (Figure 2). The manufacturer's claim of greater than 90% SWNT purity has been further confirmed by thorough TEM imaging as presented in the Supporting Information (Figure S1). The pretreatment of the as-received SWNTs resulted in debundling and shortening of SWNT clusters, which was evidenced by the decrease in the SWNT hydrodynamic radius, determined by dynamic light scattering. The average hydrodynamic radius of the SWNT clusters decreased from $149.4 \pm 2.1 \text{ nm}$ for the as-received sample to $78.1 \pm 1.7 \text{ nm}$ for sonicated SWNTs. The TEM images in Figure 2 further show multiple clustered spots that are most likely the catalyst metals used in SWNT synthesis. These catalyst clusters are occasionally present inside the nanotube bundle as well as terminal features. The ends of the SWNTs were found to have sharp edges in most cases.

Raman spectroscopy can be used to estimate SWNT diameter and also to obtain information about the CNT defect level. A typical Raman spectra of SWNTs (Figure S2 of the Supporting Information) exhibits two active Raman signature modes, namely, the radial breathing mode (RBM, near 200 cm^{-1}) and a high-energy mode (HEM or "G" band, near 1600 cm^{-1}), and another electric resonance mode originating from double resonance called the "D" band (near 1300 cm^{-1}) (34). The Raman shift frequency at the RBM mode is correlated with SWNT diameter using semiempirical relationships. The nature of SWNT samples for Raman spectroscopy necessitates that one account for bundling of SWNTs and, therefore, tube–tube interactions within the bundle (35). The following equation that accounts for bundling of SWNTs has been used to calculate SWNT diameter (d) using the RBM frequencies for the bundled state (35–37):

$$d = \frac{223.75}{\omega - 14} \quad (3)$$

where ω is the mean Raman shift at RBM peaks. The equation yielded a SWNT diameter range of 0.87–1.42 nm, using Raman shift peaks of 269.78 and 171.49 cm^{-1} . It should be noted that SWNTs were not present as individual tubes, but rather as bundles, and the bundled state is demonstrated by the Raman peak at 269.78 cm^{-1} (38, 39). The defect density in SWNTs can be estimated using the Raman response in the D band region (40). For the 1.58 eV laser, the G/D ratio is estimated to be 0.90 for untreated and 0.83 for treated SWNTs. This shows an increase in defect density due to successive sonication of the SWNT samples.

TGA data for untreated SWNTs are presented in Figure S3 of the Supporting Information. The mass loss profile (Figure S3a) shows that the major onset of oxidation

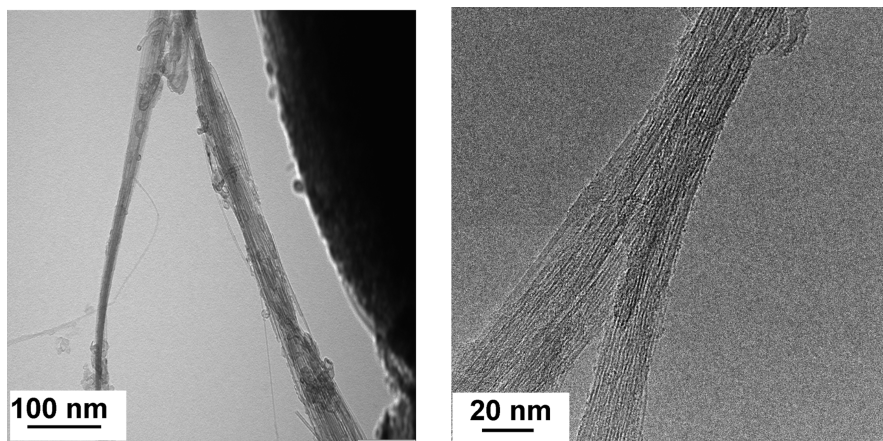


FIGURE 2. TEM images of representative SWNTs before sonication pretreatment. The sample shows long and bundled SWNTs (left) with demonstration of SWNT predominance in the sample when it is imaged at a high resolution (right).

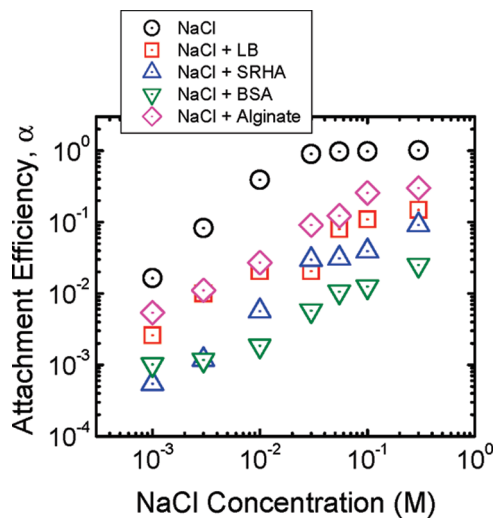


FIGURE 3. Attachment efficiencies of SWNTs as a function of NaCl concentration in the presence of various biomacromolecules and Suwannee River humic acid (SRHA). The concentration of each macromolecule was maintained at 2.5 mg/L of TOC. The attachment efficiencies are calculated by normalizing the actual aggregation rate with the favorable (fast) aggregation rate with NaCl alone. Aggregation experiments were conducted at pH 6 and room temperature (23 °C).

occurred at ~450 °C. The plateau beyond ~670 °C resulted in a residual mass of 1.8% of the total mass of the SWNT sample, which can be attributed to the catalyst metal oxide content. The derivative of the mass loss profile in Figure S3b shows that it is a single-stage oxidation with the maximum rate of oxidation (i.e., the major peak) occurring at 592 °C. The singular peak in the mass loss profile with no observable shoulders demonstrates that the SWNT sample used is relatively pure with a very small fraction of MWNTs and negligible amorphous carbonaceous material (41, 42).

SWNT Aggregation Kinetics with Monovalent (Na^+) Cations. The SWNT stability curve, i.e., the variation of the attachment efficiency (α) with the molar concentration of Na^+ (1–300 mM), is presented in Figure 3. At pH 6.0, the SWNTs exhibit strong electrostatic repulsion at low ionic strengths. In the absence of biomacromolecules and humic acid, two distinct aggregation regimes, unfavorable (slow) and favorable (fast), are observed. This observation indicates that DLVO type interactions are the dominant mechanism of SWNT stabilization, consistent with literature on aggregation of carbonaceous nanomaterials

(9, 13, 22). The critical coagulation concentration (CCC), indicated by the inflection point in the stability curve for NaCl only, occurs at approximately 20 mM NaCl. The only reported SWNT CCC value with monovalent cations in aqueous solutions was 37 mM for HNO_3 -treated SWNTs (17). The SWNTs in this study were treated with sonication, which is a mild treatment (less aggressive compared to acid etching) for stabilization of SWNTs. Therefore, the lower CCC value in this case conforms with the low EPM of the SWNTs (Figure 1) compared to that cited in the literature (17). CCC values for MWNTs with monovalent ions were reported in our previous study (25 mM NaCl) (13) and by Smith et al. (93 mM NaCl at pH 6.0) (9) for sonicated and HNO_3 -treated MWNTs, respectively. Note that CCC values for fullerene nanoparticles are much higher, ranging from 85 to 160 mM (22, 23).

The effect of biomacromolecules (alginate, LB, and BSA) and SRHA on the aggregation kinetics of SWNTs is shown in Figure 3. Overall, the presence of biomacromolecules and SRHA retards the aggregation rate of SWNTs. Among the three model biomacromolecules and the humic acid, BSA proteins have the strongest effect with respect to slowing the SWNT aggregation rate in the presence of monovalent salts, followed by SRHA, LB, and alginate. It is also observed that for the salt concentrations examined, none of the stability profiles with biomacromolecules or SRHA has reached the favorable aggregation regime (i.e., $\alpha = 1$ as for NaCl alone). This finding demonstrates that the presence of biomacromolecules and SRHA will enhance the stability of SWNTs even at high salt concentrations, thereby having significant environmental and biological implications as discussed later.

SWNT Aggregation Kinetics with Divalent (Ca^{2+}) Cations. The aggregation kinetics of SWNTs was also examined for divalent Ca^{2+} (from 0.1 to 10 mM). The attachment efficiencies of SWNTs as a function of Ca^{2+} concentration are presented in Figure 4. In the absence of biomacromolecules or SRHA, we see a DLVO type behavior similar to that observed for NaCl, with distinct unfavorable and favorable aggregation regimes. The estimated CCC value is ~2 mM CaCl_2 , 1 order of magnitude lower than that of NaCl. The SWNT CCC values have a weak dependence on counterion valence (CCC with Ca^{2+} is 10 times lower than with Na^+), which follows the Schulze–Hardy rule (17, 43) [i.e., CCC $\sim 1/z^n$ ($n = 2$ –6), with z being the counterion valence]. Previous studies report CCC values for sonicated MWNTs to be 2.6 mM CaCl_2 (13) and 1.2 mM CaCl_2 for HNO_3 -treated MWNTs (9), similar to the CCC value observed for SWNTs in this study. Higher CCC values were reported for fullerenes (4.1–6.0 mM CaCl_2) (22, 23, 44).

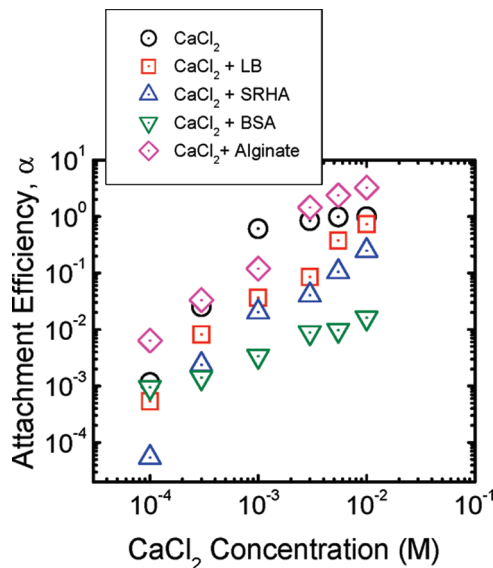


FIGURE 4. Attachment efficiencies of SWNTs as a function of CaCl_2 concentration in the presence of biomacromolecules and Suwannee River humic acid (SRHA). The concentration of each macromolecule was maintained at 2.5 mg/L of TOC. The attachment efficiencies are calculated by normalizing the actual aggregation rate with the favorable (fast) aggregation rate with CaCl_2 alone. Aggregation experiments were conducted at pH 6 and room temperature (23°C).

The effect of biomacromolecules and SRHA on the stability of SWNTs is also presented in Figure 4. The overall aggregation behavior in the presence of calcium ions with biomacromolecules and SRHA is similar to that observed with monovalent (Na^+) ions. One notable exception, however, is the enhanced aggregation of SWNTs in the presence of alginate. BSA exhibited the strongest retarding effect with a markedly flattened slope in the unfavorable regime, followed by SRHA and LB. The stability profiles in the presence of BSA, SRHA, and LB show similar trends compared to that of NaCl, with no sign of plateauing at any CaCl_2 concentration. Alginate had the weakest impact on SWNT stability, but at CaCl_2 concentrations of >3 mM, attachment efficiencies of >1 were observed. The enhanced aggregation with alginate in the presence of high calcium ion concentrations is discussed in the subsequent subsections.

Role of Biomacromolecules and Humic Acid in SWNT Aggregation. The EPM or surface charge of SWNTs changed only slightly in the presence of any of the examined biomacromolecules or SRHA (Figure 1), but the impact of biomacromolecules and SRHA on SWNT stability was very significant. This observation strongly suggests that the mechanism of stabilization for SWNTs with biomacromolecules and SRHA involves steric repulsive forces imparted by the adsorbed macromolecular layers. Similar arguments were presented for the enhanced stability of fullerene nanoparticles (23) and MWNTs (13) in the presence of SRHA. BSA proteins have had the strongest effect in retarding the SWNT aggregation rate. BSA molecules are globular proteins with a tendency to spontaneously accumulate on surfaces (45). The globular architecture of adsorbed BSA on the hydrophobic SWNT surfaces induces longer-range steric repulsive forces compared to the relatively linear LB, SRHA, and alginate macromolecules, thereby having a greater impact on retarding the SWNT aggregation rate. The structure of BSA proteins is controlled by the interplay among the hydrogen bonds between the peptide units in α -helices and the rotational freedom of the polypeptide in the β -sheets (45, 46). When a protein molecule is adsorbed to a surface,

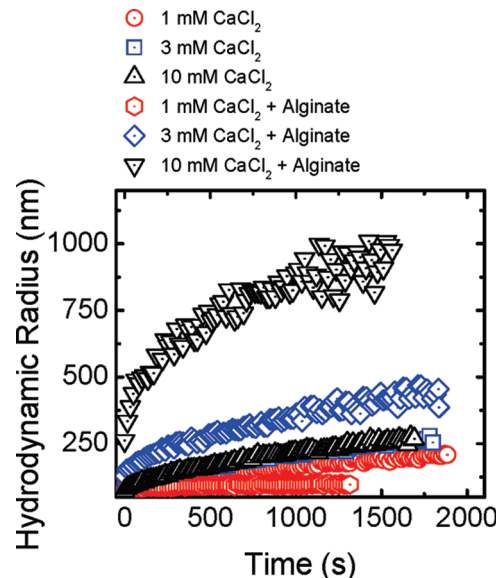


FIGURE 5. Aggregation profiles of SWNTs in various CaCl_2 solutions in the absence and presence of alginate (2.5 mg/L of TOC). Aggregation experiments were conducted at pH 6 and room temperature (23°C).

its parent structure is altered because of the surface attachment. However, it has been shown that attachment of BSA molecules on hydrophobic surfaces provides enough dehydration of the amino acids within the protein structure and thereby provides a more compact globular structure after attachment (45–47).

Enhanced Aggregation of SWNTs with Alginate in CaCl_2 Solutions. Enhanced aggregation of SWNTs was observed in the presence of high CaCl_2 concentrations, resulting in attachment efficiencies greater than unity (Figure 4). Figure 5 shows the dramatic increase in the rate of SWNT aggregation at and beyond 3 mM CaCl_2 . In the absence of alginate, the favorable (diffusion-limited) aggregation regime is attained at 3 and 10 mM CaCl_2 as these concentrations are above the CCC value for SWNTs (Figure 4 and associated discussion). However, upon addition of alginate, the slopes of the aggregation curves at 3 and 10 mM CaCl_2 are higher than the slopes without alginate, indicating aggregation rates greater than those possible for the favorable aggregation regime. Alginate molecule bridging is identified as the primary mechanism of such enhanced aggregation behavior of SWNTs with Ca^{2+} . Alginate bridging and enhanced aggregation of SWNTs are shown in the TEM image in Figure S4 of the Supporting Information. It has been previously shown that Ca^{2+} ions can cause the formation of alginate gel through bridging of alginate molecules which results in enhanced aggregation (22, 23). Enhanced aggregation due to calcium bridging has also been observed for fullerene nanoparticles in the presence of humic acid and high calcium ion concentrations (23).

Implications for Aquatic and Biological Environments. Natural aquatic environments contain monovalent and divalent salts as well as natural organic matter (humic and fulvic substances and polysaccharides). The aggregation state and fate and transport of nanomaterials in aquatic systems will be greatly influenced by their interaction with natural organic matter. Likewise, interaction of nanomaterials in biological fluids or with biological interfaces will involve association with biomacromolecules such as proteins. In studies that involve interaction of bacteria or cells with nanomaterials, culture media that contain biomacromolecules, such as Luria-Bertani (LB) broth, will interact with the nanomaterials and will play a key role in their behavior. Therefore, to predict the fate and transport

of SWNTs in aquatic environments or to understand the interaction of SWNTs with microorganisms and biological interfaces, it is imperative to have a systematic fundamental understanding of the aggregation behavior in these environments. Results from this study suggest that SWNTs can be relatively stable under solution chemistries typical of aquatic environments. The SWNT aggregation rate is significantly reduced in the presence of NOM, which is ubiquitous in aquatic environments, therefore enhancing their transport and mobility upon release. The marked effect of biomacromolecules on the aggregation behavior of SWNTs will have a significant influence on their interaction with the biological species and possibly their cytotoxicity. We note that the SWNTs used in this study were mechanically dispersed for investigating the fundamental aggregation behavior of SWNTs. This may be relevant to the biological application of SWNTs, but in other scenarios, SWNTs will be more bundled when released to the aquatic environment. Furthermore, in aquatic environments, SWNTs will most likely interact more with suspended and colloidal particles and mineral surfaces. Therefore, further aggregation studies of SWNTs in the presence of environmentally relevant particles will be greatly important.

Acknowledgments

Funding was provided by the National Science Foundation (BES 0646247). We are grateful to the late Dr. Marc Pypaert (Department of Cell Biology, Yale University School of Medicine, New Haven, CT) for taking the TEM images used in this study.

Supporting Information Available

TEM images of as-prepared SWNTs showing SWNT predominance (Figure S1), Raman spectra of SWNTs before and after sonication (Figure S2), TGA mass loss and mass loss derivative profiles for SWNTs (Figure S3), and a transmission electron microscope (TEM) image showing alginate gelation and enhanced SWNT aggregation (Figure S4). This material is available free of charge via the Internet at <http://pubs.acs.org.org>.

Literature Cited

- Cientifica "Nanotubes Report 2004," Cientifica, 2004.
- Baughman, R. H.; Zakhidov, A. A.; de Heer, W. A. Carbon nanotubes: the route toward applications. *Science* **2002**, *297*, 787–792.
- Balavoine, F.; Schultz, P.; Richard, C.; Mallouh, V.; Ebbesen, T. W.; Mioskowski, C. Helical crystallization of proteins on carbon nanotubes: A first step towards the development of new biosensors. *Angew. Chem., Int. Ed.* **1999**, *38*, 1912–1915.
- Lu, Q.; Moore, J. M.; Huang, G.; Mount, A. S.; Rao, A. M.; Larcom, L. L.; Ke, P. C. RNA polymer translocation with single-walled carbon nanotubes. *Nano Lett.* **2004**, *4*, 2473–2477.
- Chen, J.; Hamon, M. A.; Hu, H.; Chen, Y.; Rao, A. M.; Eklund, P. C.; Haddon, R. C. Solution properties of single-walled carbon nanotubes. *Science* **1998**, *282*, 95–98.
- Hyung, H.; Fortner, J. D.; Hughes, J. B.; Kim, J.-H. Natural organic matter stabilizes carbon nanotubes in the aqueous phase. *Environ. Sci. Technol.* **2007**, *41*, 179–184.
- Pompeo, F.; Resasco, D. E. Water solubilization of single-walled carbon nanotubes by functionalization with glucosamine. *Nano Lett.* **2002**, *2*, 369–373.
- Islam, M. F.; Rojas, E.; Bergey, D. M.; Johnson, A. T.; Yodh, A. G. High weight fraction surfactant solubilization of single-walled carbon nanotubes in water. *Nano Lett.* **2003**, *3*, 269–273.
- Smith, B.; Wepasnick, K.; Schrote, K. E.; Bertele, A. R.; Ball, W. P.; O'Melia, C.; Fairbrother, D. H. Colloidal properties of aqueous suspensions of acid-treated, multi-walled carbon nanotubes. *Environ. Sci. Technol.* **2009**, *43*, 819–825.
- Zheng, M.; Jagota, A.; Semke, E. D.; Diner, B. A.; McLean, R. S.; Lustig, S. R.; Richardson, R. E.; Tassi, N. G. DNA-assisted dispersion and separation of carbon nanotubes. *Nat. Mater.* **2003**, *2*, 338–342.
- Pan, H.; Liu, L.; Guo, Z.-X.; Dai, L.; Zhang, F.; Zhu, D.; Czerw, R.; Carroll, D. L. Carbon nanotubols from mechanochemical reaction. *Nano Lett.* **2002**, *3*, 29–32.
- Smith, B.; Wepasnick, K.; Schrote, K. E.; Cho, H.-H.; Ball, W. P.; Fairbrother, D. H. Influence of surface oxides on the colloidal stability of multi-walled carbon nanotubes: A structure–property relationship. *Langmuir* **2009**, *25*, 9767–9776.
- Saleh, N. B.; Pfefferle, L. D.; Elimelech, M. Aggregation kinetics of multiwalled carbon nanotubes in aquatic systems: Measurements and environmental implications. *Environ. Sci. Technol.* **2008**, *42*, 7963–7969.
- Chen, Q.; Saltiel, C.; Manickavasagam, S.; Schadler, L. S.; Siegel, R. W.; Yang, H. Aggregation behavior of single-walled carbon nanotubes in dilute aqueous suspension. *J. Colloid Interface Sci.* **2004**, *280*, 91–97.
- Giordano, A. N.; Chaturvedi, H.; Poler, J. C. Critical coagulation concentrations for carbon nanotubes in nonaqueous solvent. *J. Phys. Chem. C* **2007**, *111*, 11583–11589.
- Niyogi, S.; Boukhalfa, S.; Chikkannanavar, S. B.; McDonald, T. J.; Heben, M. J.; Doorn, S. K. Selective aggregation of single-walled carbon nanotubes via salt addition. *J. Am. Chem. Soc.* **2007**, *129*, 1898–1899.
- Sano, M.; Okamura, J.; Shinkai, S. Colloidal nature of single-walled carbon nanotubes in electrolyte solution: The Schulze–Hardy rule. *Langmuir* **2001**, *17*, 7172–7173.
- Karajanagi, S. S.; Vertegel, A. A.; Kane, R. S.; Dordick, J. S. Structure and function of enzymes adsorbed onto single-walled carbon nanotubes. *Langmuir* **2004**, *20*, 11594–11599.
- Shi Kam, N. W.; Jessop, T. C.; Wender, P. A.; Dai, H. Nanotube molecular transporters: internalization of carbon nanotube–protein conjugates into mammalian cells. *J. Am. Chem. Soc.* **2004**, *126*, 6850–6851.
- Shin, M.; Shi Kam, N. W.; Chen, R. J.; Li, Y.; Dai, H. Functionalization of carbon nanotubes for biocompatibility and biomolecular recognition. *Nano Lett.* **2002**, *2*, 285–288.
- Fadel, T. R.; Steenblock, E. R.; Stern, E.; Li, N.; Wang, X.; Haller, G. L.; Pfefferle, L. D.; Fahmy, T. M. Enhanced cellular activation with single walled carbon nanotube bundles presenting antibody stimuli. *Nano Lett.* **2008**, *8*, 2070–2076.
- Chen, K. L.; Elimelech, M. Aggregation and deposition kinetics of fullerene (C60) nanoparticles. *Langmuir* **2006**, *22*, 10994–11001.
- Chen, K. L.; Elimelech, M. Influence of humic acid on the aggregation kinetics of fullerene (C60) nanoparticles in monovalent and divalent electrolyte solutions. *J. Colloid Interface Sci.* **2007**, *309*, 126–134.
- Hu, H.; Yu, A.; Kim, E.; Zhao, B.; Itkis, M. E.; Bekyarova, E.; Haddon, R. C. Influence of the zeta potential on the dispersability and purification of single-walled carbon nanotubes. *J. Phys. Chem. B* **2005**, *109*, 11520–11524.
- Mamedov, A. A.; Kotov, N. A.; Prato, M.; Guldi, D. M.; Wicksted, J. P.; Hirsch, A. Molecular design of strong single-wall carbon nanotube/polyelectrolyte multilayer composites. *Nat. Mater.* **2002**, *1*, 190–194.
- Jiang, L. Q.; Gao, L.; Sun, J. Production of aqueous colloidal dispersions of carbon nanotubes. *J. Colloid Interface Sci.* **2003**, *260*, 89–94.
- Clougherty, D. P.; Zhu, X. Stability and Teller's theorem: fullerenes in the march model. *Phys. Rev. A* **1997**, *56*, 632.
- Leys, F. E.; Amovilli, C.; Howard, I. A.; March, N. H.; Rubio, A. Surface charge model of a carbon nanotube: Self-consistent field from Thomas–Fermi theory. *J. Phys. Chem. Solids* **2003**, *64*, 1285–1288.
- Chen, K. L.; Elimelech, M. Relating colloidal stability of fullerene (C60) nanoparticles to nanoparticle charge and electrokinetic properties. *Environ. Sci. Technol.* **2009**, *43*, 7270–7276.
- Zimmermann, R.; Dukhin, S.; Werner, C. Electrokinetic measurements reveal interfacial charge at polymer films caused by simple electrolyte ions. *J. Phys. Chem. B* **2001**, *105*, 8544–8549.
- Chen, R. J.; Zhang, Y.; Wang, D.; Dai, H. Noncovalent sidewall functionalization of single-walled carbon nanotubes for protein immobilization. *J. Am. Chem. Soc.* **2001**, *123*, 3838–3839.
- White, B.; Banerjee, S.; O'Brien, S.; Turro, N. J.; Herman, I. P. Zeta-potential measurements of surfactant-wrapped individual single-walled carbon nanotubes. *J. Phys. Chem. C* **2007**, *111*, 13684–13690.
- Liu, Y.; Gao, L.; Zheng, S.; Wang, Y.; Sun, J.; Kajiura, H.; Li, Y.; Noda, K. Debundling of single-walled carbon nanotubes by using natural polyelectrolytes. *Nanotechnology* **2007**, *18*, 365702.
- Thomsen, C.; Reich, S.; Maultzsch, J. Resonant raman spectroscopy of nanotubes. *Philos. Trans. R. Soc. London, Ser. A* **2004**, *362*, 2337–2359.

- (35) Venkateswaran, U. D.; Rao, A. M.; Richter, E.; Menon, M.; Rinzler, A.; Smalley, R. E.; Eklund, P. C. Probing the single-wall carbon nanotube bundle: Raman scattering under high pressure. *Phys. Rev. B* **1999**, *59*, 10928.
- (36) Dresselhaus, M. S.; Eklund, P. C. Phonons in carbon nanotubes. *Adv. Phys.* **2000**, *49*, 705–814.
- (37) Jishi, R. A.; Venkataraman, L.; Dresselhaus, M. S.; Dresselhaus, G. Phonon modes in carbon nanotubes. *Chem. Phys. Lett.* **1993**, *209*, 77–82.
- (38) Dyke, C. A.; Stewart, M. P.; Tour, J. M. Separation of single-walled carbon nanotubes on silica gel. Materials morphology and raman excitation wavelength affect data interpretation. *J. Am. Chem. Soc.* **2005**, *127*, 4497–4509.
- (39) Heller, D. A.; Barone, P. W.; Swanson, J. P.; Mayrhofer, R. M.; Strano, M. S. Using raman spectroscopy to elucidate the aggregation state of single-walled carbon nanotubes. *J. Phys. Chem. B* **2004**, *108*, 6905–6909.
- (40) Bockrath, M.; Liang, W.; Bozovic, D.; Hafner, J. H.; Lieber, C. M.; Tinkham, M.; Park, H. Resonant electron scattering by defects in single-walled carbon nanotubes. *Science* **2001**, *291*, 283–285.
- (41) Hu, H.; Zhao, B.; Itkis, M. E.; Haddon, R. C. Nitric acid purification of single-walled carbon nanotubes. *J. Phys. Chem. B* **2003**, *107*, 13838–13842.
- (42) Zhang, M.; Yudasaka, M.; Koshio, A.; Iijima, S. Thermogravimetric analysis of single-wall carbon nanotubes ultrasonicated in monochlorobenzene. *Chem. Phys. Lett.* **2002**, *364*, 420–426.
- (43) Elimelech, M.; Jia, X.; Gregory, J.; Richard, W. *Particle Deposition & Aggregation: Measurement, Modelling and Simulation*; Butterworth-Heinemann: Woburn, MA, 1998.
- (44) Mchedlov-Petrossyan, N. O.; Klochkov, V. K.; Andrievsky, G. V. Colloidal dispersions of fullerene C60 in water: Some properties and regularities of coagulation by electrolytes. *J. Chem. Soc., Faraday Trans.* **1997**, *93*, 4343–4346.
- (45) Norde, W. In *Physical Chemistry of Biological Interfaces*; Bazkin, A., Norde, W., Eds.; Marcel and Dekker, Inc.: New York, 1999; pp 115–135.
- (46) Norde, W.; Anusiem, A. C. I. Adsorption, desorption and re-adsorption of proteins on solid surfaces. *Colloids Surf.* **1992**, *66*, 73–80.
- (47) Norde, W.; Giacomelli, C. E. BSA structural changes during homomolecular exchange between the adsorbed and the dissolved states. *J. Biotechnol.* **2000**, *79*, 259–268.

ES903059T